ROYAL SOCIETY OPEN SCIENCE

royalsocietypublishing.org/journal/rsos

Research

Cite this article: Turvey ST *et al*. 2025 Morphometric characterization of Holocene mandibles expands the ecological baseline for understanding gibbon extinction dynamics. *R. Soc. Open Sci.* **12**: 242065.
https://doi.org/10.1098/rsos.242065

Received: 26 November 2024
Accepted: 29 May 2025

Subject Category:
Ecology, conservation, and global change biology

Subject Areas:
ecology, palaeontology

Keywords:
cao vit gibbon, conservation palaeobiology, geometric morphometrics, historical baselines, *Nomascus nasutus*, refugee species

Author for correspondence:
Samuel T. Turvey
e-mail: samuel.turvey@ioz.ac.uk

Electronic supplementary material is available online at https://doi.org/10.6084/m9.figshare.c.7851565.

THE ROYAL SOCIETY PUBLISHING

Morphometric characterization of Holocene mandibles expands the ecological baseline for understanding gibbon extinction dynamics

Samuel T. Turvey[1], Alejandra Ortiz[2,3], Matthew Granger[1], Selina Brace[4], Rasmus Amund Henriksen[5], Qingping Yang[6], Tuấn Anh Nguyễn[7], Laura T. Buck[8], Heidi Ma[1], James P. Hansford[1], Thomas Booth[4], Helen J. Chatterjee[9], Pengfei Fan[10] and Xi Chen[11]

[1]Institute of Zoology, Zoological Society of London, London, UK
[2]Department of Anthropology, New York University, New York, NY, USA
[3]Arizona State University, Tempe, AZ, USA
[4]Department of Science, The Natural History Museum, London, UK
[5]University of Copenhagen, Kobenhavn, Denmark
[6]Guangxi Institute of Cultural Relic Protection and Archaeology, Nanning, People's Republic of China
[7]Faculty of Environmental Sciences, University of Science, Vietnam National University, Hanoi, Vietnam
[8]Liverpool John Moores University, Liverpool, UK
[9]University College London, London, UK
[10]School of Life Sciences, Sun Yat-Sen University, Guangzhou, People's Republic of China
[11]Department of Cultural Heritage and Museology, Nanjing Normal University, Nanjing, People's Republic of China

STT, 0000-0002-3717-4800; SB, 0000-0003-2126-6732; JPH, 0000-0002-5702-8915; PF, 0000-0003-4747-5727

Human activities have driven biodiversity loss for millennia, and conservation of 'refugee species' that survive as remnant populations requires insights from historical baselines. However, reconstructing the past distribution and ecology of such species is challenging due to data limitations with specimen-based archives. Here, we assess the taxonomic identity of two gibbon mandibles from the Wumingshan Neolithic site in Guangxi, China. Although

ancient DNA extraction was unsuccessful, a suite of linear and geometric morphometric analyses using dental and mandibular characters reveals that these mandibles fall within or close to variation shown by extant Chinese *Nomascus* gibbons and can be assigned to the cao vit gibbon *N. nasutus*. This is now one of the world's rarest mammals, with a surviving population of 74 individuals in one site. Comparative assessment of bioclimatic, abiotic and anthropogenic parameters for Wumingshan and other sites where *N. nasutus* historically occurred reveals the species was formerly a landscape generalist but is now restricted to a high-elevation refugium with reduced human pressures. Our multidisciplinary analyses provide a new baseline on niche requirements and vulnerability for *N. nasutus* with implications for population management, demonstrating the importance of integrating environmental archives into conservation planning.

1. Introduction

Conservation of threatened species requires an evidence-based approach, where management decisions are informed by empirical data on key parameters such as species' ecological requirements [1]. Most conservation evidence utilizes recent baselines derived from ecological data-collection approaches [2,3]. However, human activities have driven biodiversity loss for millennia, meaning that conservation inferences based only upon modern states may be incomplete and biased [4]. For example, many species have experienced historical human-caused range collapse, and survive as 'refugee species' in sites that do not exhibit the full range of environmental conditions they can tolerate [5,6]. Such sites can represent ecologically suboptimal or marginal conditions where survival reflects spatial heterogeneity in threats rather than habitat quality, such as high-elevation or otherwise inaccessible refugia where human access is restricted by landscape conditions [7–9]. Using parameters associated with survival of remnant populations to guide conservation can therefore lead to erroneous assumptions about their ecological requirements and tolerance to change, and can promote conservative or inappropriate management targets. While it may not be possible to restore species to regions from which they have been extirpated (e.g. due to human-driven transformation of natural habitats), reconstructing the environmental determinants of threatened species' past distributions, and their resilience or vulnerability across different landscapes over time, can provide new predictive insights for conservation planning [10,11].

However, reconstructing the past distribution and ecology of refugee species can prove challenging. Environmental archives are available for many systems and can potentially provide insights into past biodiversity states, but these archives vary in both quantity and quality, such as in taxonomic and geographic representation and resolution [12]. Specimen-based archives are usually morphologically incomplete, and zooarchaeological and fossil samples, which often pre-date major human impacts to priority systems, typically only constitute preserved hard tissues of varying diagnostic status [13]. For species reduced to tiny surviving populations, comparative modern material is often also limited, compounding the problems of identifying historical specimens. Evaluating the conservation information-content of environmental archives for threatened species therefore requires critical appraisal of available data, often using multiple approaches.

Evidence-based conservation is particularly urgent for eastern and southeast Asia, as this biodiversity-rich region is experiencing extreme resource overexploitation and habitat conversion, and contains the world's highest proportions of threatened terrestrial vertebrates [14]. Although availability of environmental archives varies across this region, rich historical, zooarchaeological and fossil archives exist in China, which has enabled reconstruction of long-term faunal dynamics and biodiversity responses to past human pressures [15,16]. These archives have also identified several Asian mammals as refugee species that persist today in reduced areas of their former ranges, which was not apparent from modern baselines alone [17–20].

Hylobatids (gibbons and siamangs) are arboreal small apes restricted to eastern and southeast Asia, and all 20 living species are now threatened [21]. Historical records indicate that gibbons formerly occurred across eastern, central and southern China, but nearly all Chinese populations are now extinct [17]. Remnant populations of four species still persist in fragmented habitats in southwest China [22]. At least two other extant species also occurred in southwest China until the twentieth century [22], and a central Chinese species (*Junzi imperialis*) is now globally extinct [23]. Pleistocene fossils represent additional extinct Chinese species, including *Bunopithecus sericus* [24] and other taxa known only

from teeth [25]. However, the taxonomic identities and distributions of most extinct Chinese gibbons are unclear, as primates are underrepresented in Asian Quaternary archives, and morphologically diagnosable hylobatid material is unavailable from most of China [16].

Gibbons occurred in Jingxi County (Baise Municipality) and Longzhou County (Chongzuo Municipality) in southwest China's Guangxi Zhuang Autonomous Region until the 1950s, but were thought to be extinct before researchers could determine their species identity [26]. A remnant surviving population was discovered near the Chinese border in Vietnam's Cao Bang Province in 2000 and was subsequently found to extend into Guangxi in Bangliang, Jingxi County [27,28] (figure 1). This represents the only extant population of the cao vit gibbon *Nomascus nasutus*, which is historically known from other sites in southwest China and north Vietnam east of the Red River [28–30]. This species is one of the world's rarest and most threatened mammals. It is now restricted to a single *c*.50 km^2 forest patch (the Bangliang-Trung Khanh forest block) within an inaccessible karst limestone landscape. Past censuses using traditional monitoring methods estimated a population size of *c*.120 individuals, but passive acoustic monitoring in 2021 estimated a global population of only 74 individuals [31]. Establishing a robust understanding of ecological and extinction risk parameters for this refugee species, drawing upon all available lines of evidence, is thus a priority for optimal conservation planning.

During archaeological excavations in 2013–2015, two gibbon mandibles were recovered within a Neolithic midden at Wumingshan rock shelter in Longzhou County, Guangxi, *c*.85 km from Bangliang-Trung Khanh (figure 1). Their taxonomic identity is uncertain, and they may represent either a known extant or unknown extinct gibbon. To determine the identity of these mandibles and assess what conservation-relevant information they can provide, we attempted ancient DNA extraction, conducted geometric morphometric analyses with a comparative dataset of modern and extinct hylobatids, and conducted environmental analyses to identify ecological differences associated with gibbon survival and extinction. Our combined results establish a new baseline for understanding past gibbon diversity and extinction risk, and promote the importance of using multiple complementary approaches to integrate insights from historical archives into real-world conservation problems.

2. Material and methods

2.1. Collection locality and material

Wumingshan is a 5 m wide and 20–30 m high rock shelter below a limestone cliff beside the Zuojiang River, one of a series of adjacent middle Holocene archaeological sites along this river section [32]. Accelerator mass spectrometry (AMS) dating of charcoal provides an age of 4475 ± 25 BP (Peking University ^{14}C laboratory, lab number BA141169; IntCal20 calibrated date 5287–4978 BP). The Wumingshan midden contains a diverse faunal assemblage of 1626 specimens, which also includes goral, sambar and sika deer, giant and Reeves's muntjacs, wild boar, dhole, masked and Owston's palm civets, otter, stump-tailed macaque, brush-tailed porcupine, bamboo rat, python, turtle and fish, but lacks domesticated animals [33].

The gibbon mandibles are held in the Zooarchaeology Laboratory of Nanjing Normal University (figure 1). One specimen (GLW-15) is an incomplete left mandibular corpus with m1–3 and part of the mandibular ramus. The other specimen (GLW-16) is an incomplete right mandibular corpus with pm4, m1–2, and pm3 alveolus.

2.2. Genetic analysis

All pre-PCR laboratory work was conducted in the dedicated ancient DNA laboratory at the Natural History Museum, London. Bone powder (*c*.15 mg) was removed from each sample using a handheld drill (Foredom) at slow speed. DNA extraction followed the protocol of [34] with modifications: Zymo-Spin V columns were replaced with Roche High Pure Viral Nucleic Acid Large Volume spin columns, and two final elution steps of 50 µl TET buffer (total 100 µl) were performed. Dual-indexed libraries were constructed based on [35,36]. Libraries were sequenced on an Illumina NextSeq 500, producing 76-basepair paired-end reads, and were sent for mitochondrial enrichment capture at Arbor BioSciences using the myBaits® MegaMito kit and sequenced on a NovaSeq S4 paired-end 150.

Sequencing reads were processed identically for both samples. Raw paired-end sequencing files were trimmed and quality-filtered using standard aDNA protocols [37]. An iterative mapping process

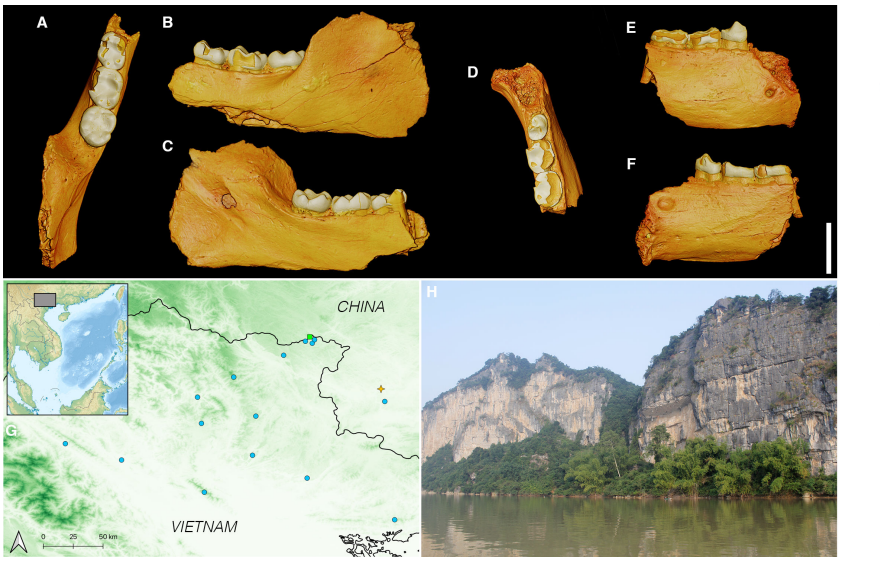

Figure 1. A–F, three-dimensional surface models of Wumingshan mandibles generated from micro-CT scan data. A–C, GLW-15 in occlusal, buccal and lingual views. D–F, GLW-16 in occlusal, buccal and lingual views. G, Map of southwest China and north Vietnam, showing location of Bangliang-Trung Khanh (green square), localities where *Nomascus nasutus* was extirpated in the twentieth century (blue circles), and Wumingshan (yellow star). H, Wumingshan archaeological site.

was performed to reduce potential ascertainment bias, by conducting two independent analyses performing single-end alignment of merged trimmed reads of each sample to two different reference panels. Alignments and filtering procedures were performed using the software, commands and parameters reported in [37]. The first reference panel contained comparative full mitogenomes for all four hylobatid genera (*Hoolock*, $n = 1$; *Hylobates*, $n = 7$; *Nomascus*, $n = 4$; *Symphalangus*, $n = 1$), and the second contained six cytochrome *b* (cyt*b*) sequences, representing species from the mitogenome panel to which the samples successfully aligned reads after filtering (electronic supplementary material, table S1).

2.3. Morphometric analysis

To generate three-dimensional surfaces for analysis, the mandibles were scanned using a Nikon Metrology XT H 225 ST high-resolution micro-CT scanner at the Cambridge Biotomography Centre (University of Cambridge, UK) using X-Tek software (Nikon Metrology, Tring, UK). Scan parameters were: tungsten target; 0.5 mm copper filter; 120 kV; 195 mA; 1080 projections; 2 frames/projection with 1000 ms exposure. Resulting isotropic voxels were 0.017 mm^3. Micro-CT data were reconstructed using CT-PRO 3D software (Nikon Metrology) and exported as an image (.tif) stack. Reconstructed micro-CT images were imported into Avizo (Thermo Fisher Scientific TM) and segmented using semi-automatic watershed and manual editing tools. Triangle-based surface models of tooth and bone tissues were generated using the unconstrained smoothing algorithm.

The Wumingshan specimens were compared against a large morphometric dataset of hylobatid mandibles and teeth, comprising 411 modern specimens representing 19 of the 20 extant species and all four extant genera (mean of 21.4 specimens per species, range = 1–73), three modern specimens only referrable to genus (*Hoolock* sp., $n = 2$; *Nomascus* sp., $n = 1$), and single specimens of the extinct Chinese taxa *Bunopithecus sericus* and *Junzi imperialis*. Data were collected from photographs and surface CT and micro-CT scans (electronic supplementary material, table S2). Three-dimensional digital models were oriented following the same protocols as those used for photographing original skeletal specimens, with no significant differences between data derived from digital photographs and from screenshots of three-dimensional models [23]. Sex is unknown for the Wumingshan specimens, so this variable was not included in analysis. However, gibbons do not exhibit significant sexual dimorphism in skull or dental morphology [38,39].

Taxonomic affinities of the Wumingshan specimens were investigated using two-dimensional linear measurements of molar crown size and mandibular corpus robusticity, and two-dimensional geometric morphometrics of molar crown outline and occlusal shape and mandibular corpus shape. Comparative data were collected on left mandibles and teeth when available, and metrical and shape analyses were

performed exclusively on adult individuals with m3 in occlusion and no pathology. Analyses were specifically chosen to accommodate limitations arising from tooth wear or damage, and reconstruction of worn/chipped teeth and criteria for determining whether a tooth could be included in different analyses followed well-established protocols [40,41]. Analysis of crown and cervical tooth outlines with moderate to pronounced wear is less prone to misleading outcomes, whereas overall occlusal morphology is more affected by wear [42–44]: occlusal morphology analysis thus included only less worn teeth (wear stages < 2 of [45]), and more worn/damaged teeth (wear stages > 3) were only included in crown outline and metric analyses. In cases of missing or heavily damaged bone or teeth, the right antimere was used and digitally mirror-imaged (this was also conducted for GLW-16 to enable direct comparison with our dataset). Despite these protocols, each Wumingshan specimen could only be included in some analyses (electronic supplementary material, table S2).

For analysis of molar linear size data, photographs and screenshots of lower molars were collected and aligned following established protocols [24,25,46]. Standard m1–3 mesiodistal and maximum buccolingual measurements were made in Adobe Photoshop v.2.0 from scaled standardized digital images [38,47]. Except for *Hylobates klossii* m1 data [38], all data were collected by AO for consistency. Measurement data were investigated using bivariate plots of log-transformed data for individual teeth and between-group principal component analysis (bgPCA [48]) for combined m1–m2 data. Under bgPCA, the extant hylobatid sample was divided into four *a priori* genus-level groupings (*Hoolock*, *Hylobates*, *Nomascus*, *Symphalangus*). Fossil/zooarchaeological specimens were treated as additional specimens of unknown *a priori* grouping, with their location in shape space plotted *a posteriori* on bgPC1 and bgPC2.

For analysis of molar crown outline, TpsDig [49] was used to digitize 79 equally linearly spaced points along the outline, which were slid along their curve using the criterion of minimization of bending energy [50] (electronic supplementary material, figure S1). As hylobatids exhibit considerable overlap in outline shape at species and genus level when first, second and third molars are analyzed independently [25], intra-individual outline data from m1–2 and m1–3 were combined in separate analyses to enable identification of more diagnostic shape differences across taxa (m1–2 analysis included GLW-15 and GLW-16; m1–3 analysis only included GLW-15, as m3 is not preserved in GLW-16).

For analysis of crown occlusal shape, 14 homologous landmarks were placed at tips of main cusps and intersections of main grooves and crests (electronic supplementary material, figure S1). These landmarks are useful in hominin systematics and for distinguishing various stem and crown catarrhine taxa [47,51]. Analysis only included GLW-15, as pronounced tooth wear has obliterated the occlusal morphology (e.g. cusp position, fissure pattern) of the GLW-16 molars.

Mandibular analyses followed [52]. To analyse corpus robusticity, linear height and breadth data were measured at mandibular cross-section between m1 and m2 and investigated using bivariate plots of log-transformed data. For analysis of corpus shape, cross-sectional shape between m1 and m2 was quantified by digitizing three landmarks: points on alveolar border between m1 and m2 on lingual side (landmark 1) and buccal side (landmark 2), and inferior-most point on corpus between m1 and m2 (landmark 3). Forty additional semi-landmarks were placed along the corpus outline (20 semi-landmarks between landmarks 1 and 3; 20 semi-landmarks between landmarks 2 and 3) (electronic supplementary material, figure S1). Landmarks and semi-landmarks were digitized in Avizo from scans of mandibles with little to no damage, with semi-landmarks slid along their curve using the criterion of minimization of bending energy [53]. Analyses only included GLW-16, as the mandibular body of GLW-15 is not preserved at the level of m1–m2.

For geometric morphometric analyses, coordinate data were imported into MorphoJ v.107a [54] and superimposed using generalized Procrustes analysis for conversion into shape variables. Shape variation was investigated using PCA and bgPCA, with wireframe models created to visualize extreme configurations and determine aspects of shape most correlated with PC1 and PC2. Procrustes distances were calculated at genus and species levels using principal component coordinates. Given small sample sizes for some taxa, bgPCA was not performed for combined m1–2 and m1–3 outline analyses, and m2 and m3 occlusal shape analyses were conducted at the genus level. Allometry was tested using multivariate regression of Procrustes coordinates (dependent variables) versus log centroid size (independent variable). Analyses were performed in MorphoJ, PAST v.4.07b [55] and R v.4.0.2 [56] using the packages Geomorph [57] and Morpho [58].

2.4. Environmental analysis

Locality records were obtained for extirpated *Nomascus nasutus* populations in southwest China and north Vietnam, with local last-occurrence dates from the 1960s–2000s [28–30,59] (n = 16; figure 1, electronic supplementary material, table S3). Other regional records that may represent *N. nasutus*, including nearly all Chinese records, were excluded due to (i) non-specific localities (e.g. reported only at county, municipality or province level) in twentieth-century or older reports [15,17,26]; (ii) taxonomic uncertainty [29]; (iii) morphometric analysis indicating that Pleistocene fossils from Guangxi probably represent a distinct, now-extinct species [25].

Data were collected on environmental conditions (bioclimatic, abiotic, anthropogenic) for Bangliang-Trung Khanh, historical *N. nasutus* localities and Wumingshan. Climate data for 1970–2000 were obtained from Bangliang-Trung Khanh and historical localities at *c*.1 km (0.5 arc-minute) resolution from WorldClim v.2.1 [60], and mid-Holocene (Northgrippian) climate data for Wumingshan were obtained at *c*.5 km resolution from PaleoClim v.1.0.1 [61]. Elevation data were obtained at 90 m resolution from the SRTM Digital Elevation Model [62], and slope data were calculated from this dataset using the 'terra' package in R v.4.4.0. Geology data were obtained from the Global Lithological Model [63], with 16 geology types converted from vectors into separate percentage-cover rasters. Global Human Footprint (GHF) data for 1995–2004 were obtained at 1 km resolution [64]. All layers were reprojected into ESRI:102028-WGS 1984 Albers Equal Area for Southern Asia to standardize pixel areas, resampled to 50 km^2 to match the approximate area occupied by the surviving *N. nasutus* population [30], and aligned. Geology layers containing fewer than three datapoints were removed. Variables were tested for multicollinearity using variance inflation factors (VIF), with removal of one of each pair of variables with a VIF score above 7 (the variable from each pair that was also correlated with more additional variables was removed). The final dataset contained five bioclimatic variables (BIO2: Mean Diurnal Temperature Range; BIO4: Temperature Seasonality; BIO12: Annual Precipitation; BIO15: Precipitation Seasonality; BIO18: Precipitation of Warmest Quarter), elevation, slope, geology and GHF. For historical records from protected areas above 50 km^2 in areas with no further locality details, environmental values were averaged across all pixels within the area.

A minimum convex polygon was made around all records, with a 50 km buffer. Comparative data on environmental conditions were sampled for all pixels lacking gibbon records within this polygon (n = 1848). Abiotic and GHF values for all sites where *N. nasutus* has been extirpated (twentieth-century sites and Wumingshan) were compared with values for pixels lacking gibbon records using two-tailed two-sample t-tests, and values for Bangliang-Trung Khanh were compared with values for background points using two-tailed one-sample t-tests. All environmental values for Bangliang-Trung Khanh and Wumingshan were also compared with values for other combined *N. nasutus* sites using two-tailed one-sample t-tests. Statistical significance was set at p = 0.0025 following Bonferroni correction. Following standardization of variables, a PCA was also conducted to investigate how modern, historical and zooarchaeological *N. nasutus* sites are distributed in environmental niche space in relation to background points.

3. Results

3.1. Genetic analysis

Unfortunately, neither specimen yielded sufficient DNA to enable downstream analysis. After duplicate removal, GLW-15 had only 0–17 aligned reads to the reference mitochondrial genomes and 1–2 aligned reads to the cyt*b* reference panel, and GLW-16 had only 1–8 and 0 aligned reads, respectively.

3.2. Morphometric analysis

The Wumingshan specimens are characterized by lower molars with subrectangular crowns (mesiodistally longer than broad), with peripherally placed cusps and limited to moderate buccolingual waisting along the mesiodistal axis. The buccal cusps are slightly mesial to the lingual cusps, and the hypoconulid is buccocentrally located relative to the crown longitudinal midline. The protoconid and hypoconid are low and rounded, and the metaconid and entoconid are more elevated and pyramidal-shaped. The metaconid is the largest cusp in all molars, followed by the protoconid and

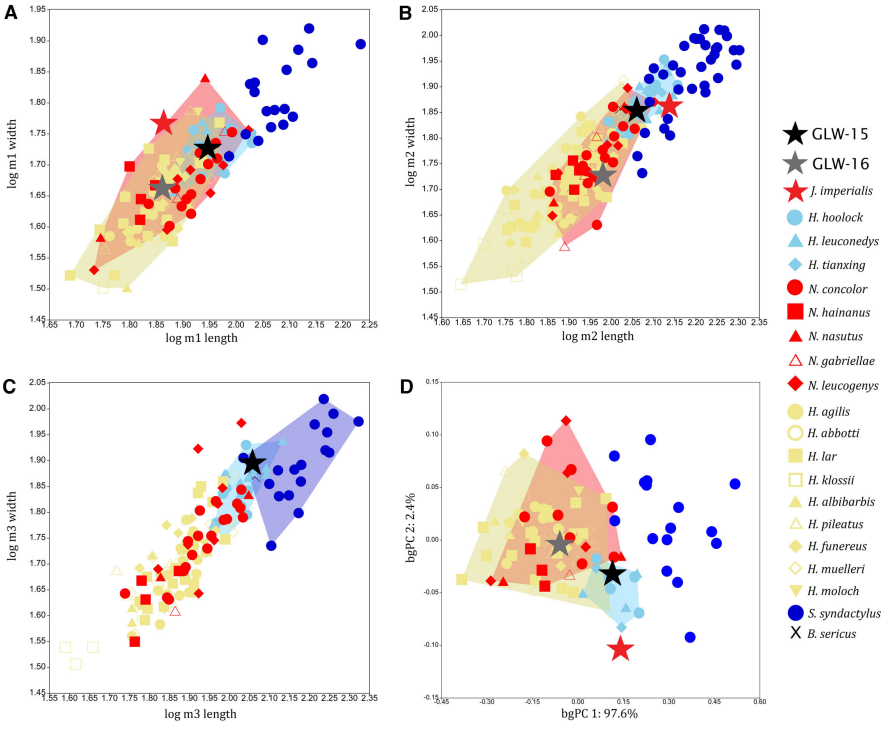

Figure 2. Bivariate plots of log-transformed lower molar crown mesiodistal length against buccolingual width: A, m1 (including GLW-15 and GLW-16); B, m2 (including GLW-15 and GLW-16); C, m3 (including GLW-15 only). D, bgPCA of combined m1-m2 measurement data (only specimens with both m1 and m2 included, including GLW-15 and GLW-16). Plots show convex hulls of extant hylobatid taxa that overlap with Wumingshan specimens.

hypoconid, which are approximately equal in size. The lingual cristids are sharper than the buccal cristids, and the hypoprotocristid and hypometacristid are well-defined. The crown outline shows well-rounded corners, with symmetrical mesial arching of the preprotocristid and premetacristid. The mesial fovea is rectangular and intermediate in size, whereas the distal fovea is smaller and ill-defined. There is no trace of a buccal cingulid. A simple Y-groove pattern is present. The basin is smooth and expansive with no wrinkling. The buccal and lingual walls are bulging, and the m3 shows minimal distal tapering. The mandible exhibits a tall, narrow corpus that tapers inferiorly and extends laterally. Tooth measurements in comparison to other hylobatids are given in electronic supplementary material, table S4.

When molar length is plotted against width, GLW-15 m1 and m2 fall within the variation range of *Hoolock*, *Hylobates* and *Nomascus*, GLW-16 m1 and m2 fall within *Hylobates* and *Nomascus*, and GLW-15 m3 falls within *Hoolock* and *Symphalangus*. For bgPCA of combined m1–m2 measurement data, GLW-15 falls within *Hoolock* and is also close to both *Hylobates* and *Nomascus*, and GLW-16 falls within *Hylobates* and *Nomascus* (figure 2) (electronic supplementary material, table S5).

In analyses of combined m1–m2 outline data, GLW-15 falls within genus-level variation of *Hoolock* and *Nomascus*, and species-level variation of *N. leucogenys*; and GLW-16 falls within genus-level variation of *Hylobates* and *Nomascus*, and species-level variation of *Ho. leuconedys* and *N. hainanus* (figure 3A,B). For combined m1–m3 outline data, GLW-15 falls exclusively within genus-level variation of *Nomascus*, and species-level variation of *N. concolor* and *N. hainanus* (figure 3C). When all principal components are considered, average combined pairwise Procrustes distances for GLW-15 m1–2 are closest to *Ho. hoolock*, *N. hainanus* and *N. nasutus*, GLW-15 m1–3 are closest to *N. hainanus*, *Ho. hoolock*, *N. nasutus*, *N. concolor* and *N. leucogenys*, and GLW-16 m1–2 are closest to *Ho. hoolock*, *Ho. leuconedys*, *N. nasustus* and *N. hainanus*. Most permutation tests for between-group Procrustes distances differentiate between extant hylobatids, but distances of GLW-15 and GLW-16 with extant groups are non-significant (electronic supplementary material, table S5). Relationships between Procrustes coordinates and log centroid size are all significant ($p < 0.05$), with size explaining 1.94, 2.46 and 3.84% of shape variance for m1, m2 and m3, respectively.

In molar occlusal shape analyses including GLW-15, m2 falls within the variation range of all four extant hylobatid genera in standard PCA and within *Hylobates*, *Hoolock* and *Nomascus* in bgPCA (figure 4A,B), and m3 falls within *Hylobates*, *Hoolock* and *Nomascus* in PCA and exclusively within

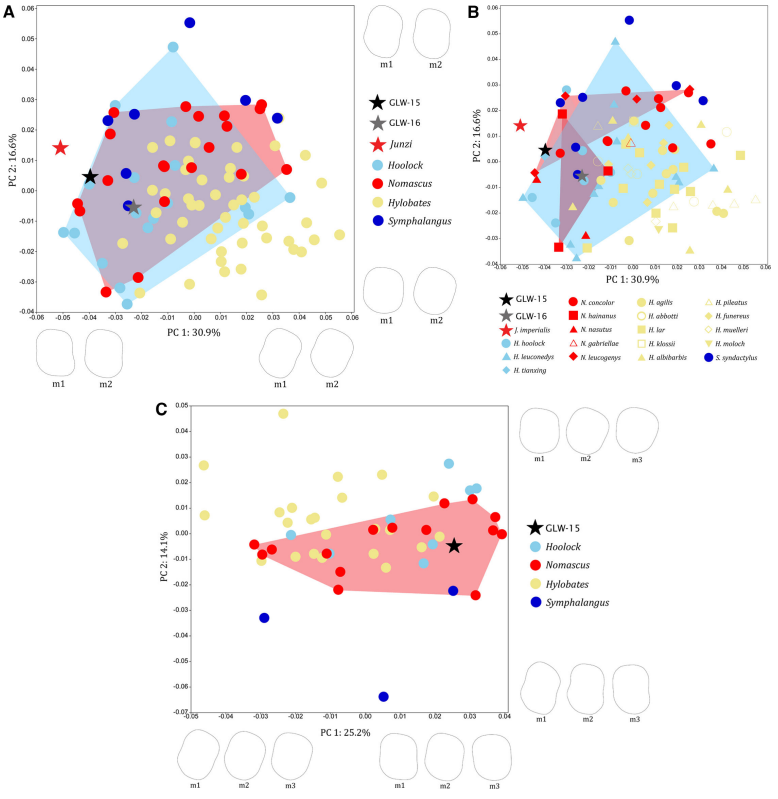

Figure 3. PCAs of combined lower molar crown outline data. A, genus-level variation in m1–m2 (including GLW-15 and GLW-16); B, species-level variation in m1–m2 (including GLW-15 and GLW-16); C, genus-level variation in m1–m3 (including GLW-15 only). Plots show convex hulls of extant hylobatid taxa that overlap with Wumingshan specimens. Wireframes illustrate shape changes of m1–m2 and m1–m3 crown outline along PC1 and PC2 in occlusal view (left molars depicted, lingual aspect to the right).

Nomascus in bgPCA (figure 4C,D). Although most permutation tests for between-group Procrustes distances differentiate between extant hylobatids, distances for GLW-15 m2 and m3 occlusal shape are non-significant, but show closest affinities to *Nomascus* (electronic supplementary material, table S5). Relationships between Procrustes coordinates and log centroid size are all significant ($p < 0.05$), with size explaining 5.25% of shape variance for m2 and 8.35% for m3.

In mandibular analyses, GLW-16 falls within the variation range of *Hoolock* and *Nomascus* for robusticity (figure 5A). Corpus shape variation shows considerable between-group overlap along the first two principal components, with GLW-16 falling within *Hylobates* and *Nomascus* at the genus-level within PCA; within *Hy. funereus* and *Hy. lar* and close to *Ho. leuconedys*, *N. nasutus* and *S. syndactylus* at the species-level within PCA; and within *Ho. leuconedys*, *Hy. lar*, *N. concolor* and *N. leucogenys* at the species level within bgPCA (figure 5B–D). GLW-16 exhibits negative scores along PC1 (47.7% of variance, associated with taller corpus that is relatively narrower throughout cross-section) and PC2 (22.1% of variance, associated with corpus of intermediate width tapering inferiorly towards buccal/lateral). Most permutation tests for between-group Procrustes distances in corpus shape differentiate between extant hylobatids; GLW-16 shows the closest distance to *Nomascus*, and specifically *N. nasutus* (electronic supplementary material, table S5). The relationship between Procrustes coordinates and log centroid size is non-significant across the sample, with size explaining only 1.01% of shape variance ($p = 0.0744$), but is significant for within-genus variation, with size explaining 1.25% of variance ($p < 0.05$).

3.3. Environmental analysis

Sites where *N. nasutus* has been extirpated do not differ from background points in elevation ($p = 0.283$), slope ($p = 0.069$) or GHF ($p = 0.781$). Conversely, Bangliang-Trung Khanh differs significantly from background points in elevation (Bangliang-Trung Khanh mean: 786.7 m, background mean: 417.8 m, $p < 0.0001$), slope (Bangliang-Trung Khanh mean: 25.2 degrees, background mean: 14.3 degrees, $p < 0.0001$) and GHF (Bangliang-Trung Khanh mean: 25.3, background mean: 33.2, $p < 0.0001$). Only 1.8%

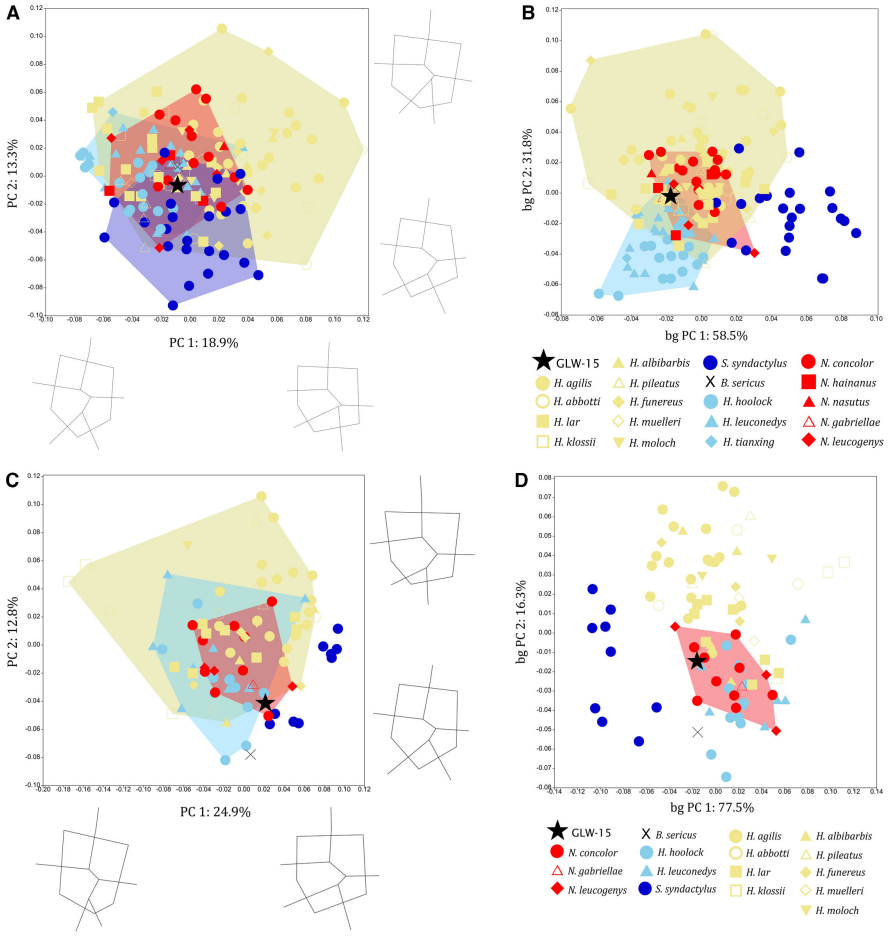

Figure 4. Analyses of species-level variation in lower molar occlusal shape, including GLW-15 only: A, m2 PCA; B, m2 bgPCA; C, m3 PCA; D, m3 bgPCA. Plots show convex hulls of extant hylobatid taxa that overlap with GLW-15. Wireframes illustrate shape changes of m2 (A) and m3 (C) occlusal shape along PC1 and PC2 in occlusal view (left molars depicted, lingual aspect to the right).

of background points show combined values of the same or higher elevations and slopes and same or lower GHF.

Compared to sites where *N. nasutus* survived until recent decades (Bangliang-Trung Khanh and twentieth-century sites), Wumingshan differs in all bioclimatic variables except BIO2 (BIO4, Wumingshan mean: 6121.3, other sites mean: 4799.3, $p < 0.0001$; BIO12, Wumingshan mean: 1269.4, other sites mean: 1644.0, $p < 0.0001$; BIO15, Wumingshan mean: 76.2, other sites mean: 85.0, $p < 0.0001$; BIO18, Wumingshan mean: 616.6, other sites mean: 928.1, $p < 0.0001$). Wumingshan also differs from sites where *N. nasutus* survived later in elevation (Wumingshan mean: 114.7 m, other sites mean: 534.6 m, $p < 0.0001$) and slope (Wumingshan mean: 1.99, other sites mean: 19.2, $p < 0.0001$), but with no difference in GHF ($p = 0.183$). Compared to sites where *N. nasutus* is extirpated (twentieth-century sites and Wumingshan), Bangliang-Trung Khanh does not differ in bioclimatic variables, but differs in elevation (modern site mean: 786.7 m, other sites mean: 497.3 m, $p = 0.0008$), slope (modern site mean: 25.2, other sites mean: 17.9, $p = 0.001$), and GHF (modern site mean: 25.3, other sites mean: 32.7, $p = 0.0002$). Bangliang-Trung Khanh and Wumingshan are both entirely composed of carbonate sedimentary rock, whereas other *N. nasutus* sites generally contain less carbonate sedimentary rock (mean: 64.8%, range: 0–100%) and more mixed sedimentary rock (mean: 22.8%, range: 0–96%).

In PCA, the first three principal components have eigenvalue scores above 1 and together account for 71.4% of total environmental variation across locality points (PC1, 33.6%; PC2, 22.0%; PC3, 15.8%). Wumingshan is separated from all modern and historical gibbon localities along PC1, where the greatest loadings (>0.4) are associated with the bioclimatic variables BIO18 (0.501), BIO12 (0.470), BIO15 (0.451) and BIO4 (−0.424). Wumingshan is associated with lower precipitation amount and seasonality, lower diurnal temperature range, and higher temperature seasonality along PC1. Bangliang-Trung Khanh is situated just outside all other gibbon localities along PC2, where the greatest loadings are instead associated with landscape structure (slope: −0.459; presence of carbonate sedimentary rock:

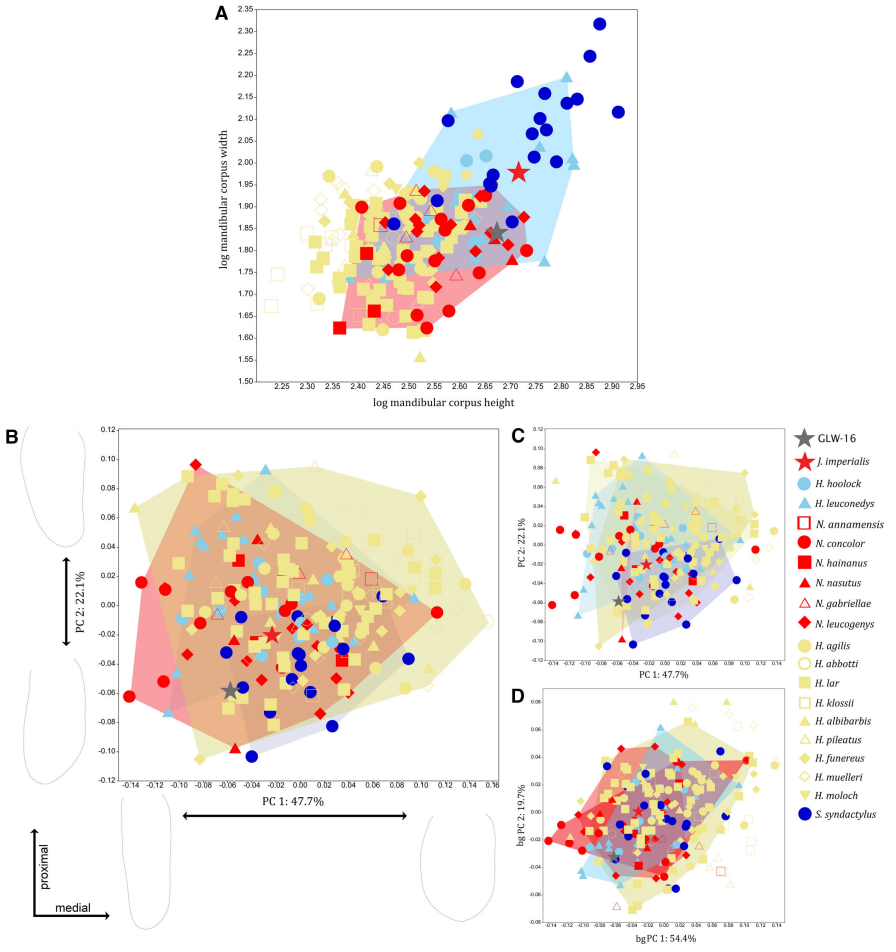

Figure 5. Analyses of mandibular shape, including GLW-16 only. A, bivariate plot of log-transformed mandibular corpus height against corpus width. B–D, analyses of variation in mandibular corpus shape: B, genus-level PCA; C, species-level PCA; D, species-level bgPCA. Plots show convex hulls of extant hylobatid taxa that overlap with GLW-16.

−0.452; elevation: −0.451) and GHF (0.446). Bangliang-Trung Khanh is associated with higher slope, more carbonate sedimentary rock, higher elevation, and lower GHF along PC2 (figure 6). Neither Wumingshan nor Bangliang-Trung Khanh are well-differentiated from other gibbon localities along PC3, where the greatest loadings are associated with presence of mixed sedimentary rock (−0.671) or carbonate sedimentary rock (0.501) (electronic supplementary material, figure S2).

4. Discussion

4.1. Taxonomic assignment of Wumingshan mandibles

Molecular evidence was unfortunately unavailable to make taxonomic inferences, and our morphometric analyses of molar and mandibular characteristics provided differing signals and resolutions for the taxonomic affinities of the Wumingshan mandibles. In most analyses, both specimens fell within the variation range for two and sometimes three extant hylobatid genera, and GLW-15 fell within the variation of all extant genera in m2 occlusal shape analysis.

It is possible that this reduced discriminatory ability reflects limited phylogenetic differentiation in dental and mandibular morphology across hylobatids (at least for the regions preserved in our specimens), or conflicting morphological patterns associated with evolutionary convergence as well as evolutionary history. Hylobatids represent a recent evolutionary radiation, with all extant genera having diverged *c*.5 million years ago [65], and with species-level divergences from the Late Pliocene to Late Pleistocene [66]. Hylobatid taxonomy has undergone substantial recent revision at both species and genus levels [67–69], with species largely differentiated on soft-tissue characteristics (e.g. pelage

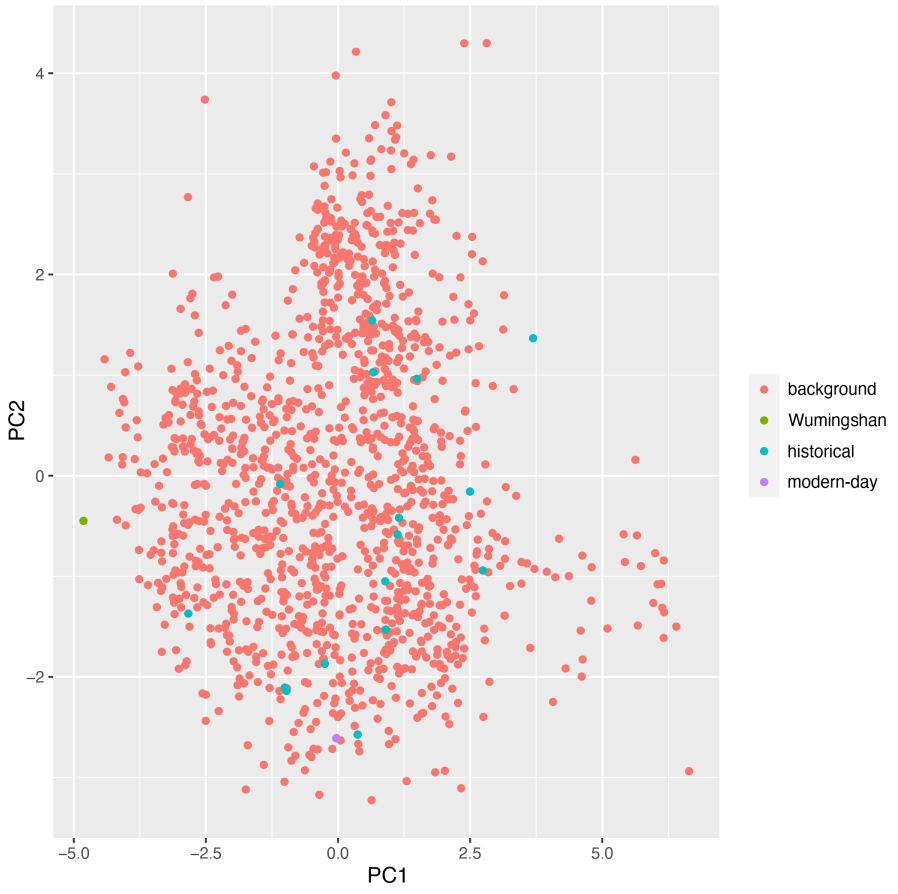

Figure 6. Principal component analysis (PC1-PC2) of modern, historical and zooarchaeological *N. nasutus* localities in environmental niche space (including bioclimatic, abiotic and anthropogenic variables) in relation to background points.

coloration) and behavioural characteristics (e.g. vocalizations) rather than external or skeletal measurement data [67,70]. Craniodental characteristics are also influenced by both phylogeny and functional adaptation [71,72], and although geometric morphometric analysis of primate molar shape demonstrates a strong phylogenetic signal at higher taxonomic levels [73], between-species morphological differences across primates are often obscured by homoplasy associated with variation in adaptive dietary ecology [74–76]. Although hylobatids are mainly ripe-fruit specialists that use figs as fallback resources, different taxa vary in their fruit-pulp specialism, fig-eating and folivory, such as across habitats with varying seasonality [77], indicating the potential for functional variation in dental and mandibular characteristics [78,79].

Whereas molar metrics can successfully differentiate between genera, species and subspecies of great apes [80], comparable studies have been unable to differentiate reliably between hylobatid taxa, especially at lower taxonomic levels [81,82]. Landmark-based shape analysis has shown that mandibular corpus outline carries a strong taxonomic signal among large-bodied apes [52], which can be of great value when dealing with fragmentary material such as the Wumingshan mandibles. However, the usefulness of the ratio of corpus breadth and height for capturing mandibular morphology in hominoids and other primates has been questioned due to positive allometry [83,84], and this approach also only captures variation in cross-sectional shape of a complex three-dimensional anatomical structure. Indeed, differentiation among hylobatid genera on the basis of mandibular corpus morphology alone appears to be particularly challenging, as all hylobatid species show gracile cross-sections [84]. Despite these limitations, craniodental morphometric analyses using large multi-character datasets have demonstrated that gibbon genera and species can be differentiated statistically, despite overlap in trait variation across morphospace [23–25,69]. Indeed, our approach to combine data for multiple molars from the same individuals in crown outline analyses is shown to improve sensitivity for differentiating hylobatid taxa [25]. Previous geometric morphometric investigations also show that two-dimensional datasets can have better species-level discrimination than three-dimensional datasets for primate molar analysis. This may be because cusp height is associated with homoplastic between-

species differences in foraging ecology and thus risks obscuring high-resolution phylogenetic signal [85], or alternately because adding a third dimension decreases the signal-to-noise ratio.

We therefore consider that the reduced discriminatory ability of our analyses is instead probably caused by sampling error associated with small sample sizes, reflecting the fact that many extant hylobatids are poorly represented in museum collections due to their rarity and/or historical inaccessibility of their habitats, and providing a limited understanding of dental and mandibular variation. Data limitation is particularly problematic for species that occur in southwest China (*Ho. tianxing*, *N. hainanus*, *N. nasutus*), and for understanding morphometric variation across *Nomascus*, for which one of the seven species is absent from our dataset (*N. siki*), and four are represented by only 1–6 individuals (*N. annamensis*, *N. gabriellae*, *N. hainanus*, *N. nasutus*). These limited samples are also not necessarily uniform in size or morphology. Although mammal species are often identifiable using cranial geometric morphometrics even with relatively small sample sizes, taxonomic assignment errors are frequent with fewer specimens, and primates in particular are prone to inaccuracies [86]. Sample sizes of over 20 individuals per species have thus been recommended to capture intraspecific variation [86]. Taxonomic uncertainty is also shown in morphometric attempts to identify zooarchaeological primate material using limited modern comparative samples [85].

Despite the unavoidable shortcomings of this data limitation, our study represents the best attempt to identify the Wumingshan mandibles, by conducting multiple analyses using dental and mandibular characters and both linear and geometric morphometric frameworks. Our results demonstrate that, while morphometric relationships to other genera differ across analyses, the specimens almost always fall within or very close to variation shown by our available *Nomascus* sample in genus-level analyses, and sometimes within *Nomascus* to the exclusion of other genera (m1–m3 molar outline analysis; m3 occlusal shape bgPCA). Furthermore, both specimens fall within or very close to Chinese *Nomascus* species (*N. concolor*, *N. hainanus*, *N. leucogenys*, *N. nasutus*) in all species-level analyses. Despite the fact that the spread of *Nomascus* in morphospace is probably artificially limited by the very small samples of most species, both Wumingshan specimens exhibit a close relationship to this genus across almost all analyses, and the balance of evidence indicates that they can both be assigned to *Nomascus*. Specifically, they share the following characteristics with *Nomascus*: (i) subrectangular molars that are fairly symmetrical (rather than skewed) along the longitudinal axis; (ii) limited waisting and no distal tapering; (iii) intermediate-sized molars with moderate to pronounced size differences between m1 and m2, and with m3 larger than m2; (iv) protoconid and hypoconid set slightly mesial relative to metaconid and entoconid, respectively (GLW-15); (v) a buccocentrally located hypoconulid relative to longitudinal midline of crown (GLW-15); (vi) a tall and narrow mandibular corpus that tapers inferiorly and laterally (GLW-16). While each characteristic might also be present in other hylobatids, especially *Hoolock* species, this combination occurs almost exclusively in *Nomascus*. The GLW-16 mandibular corpus in particular is strikingly similar to the condition seen in modern *N. nasutus* specimens.

Although some Asian landscapes support multiple co-occurring hylobatid genera, species within each genus have non-overlapping distributions, with allopatric ranges delimited by river systems or other barriers, and with only one *Nomascus* species present in any landscape [67,87]. Wumingshan is within the known historical distribution of *N. nasutus* (figure 1), and close to Longgang National Nature Reserve, where the species persisted into the twentieth century [29]. While it is difficult to be fully confident about the species-level diagnosis of the Wumingshan mandibles based upon morphology alone, we therefore refer both specimens to *N. nasutus* based upon the evidence provided by both morphology and biogeography.

4.2. Spatiotemporal extinction dynamics and ecological refugia

Today, *N. nasutus* survives as a tiny population in one geographically restricted location, meaning that conservation planning based solely upon modern-day data cannot determine the species' wider range of ecological tolerances, or contextualize whether environmental conditions within this refugium are ecologically optimal or marginal. We were unable to investigate vegetational characteristics directly between Bangliang-Trung Khanh and sites where *N. nasutus* has been lost, due to potential change in forest structure and landscape conditions at other sites through human activity and Holocene climatic shifts [61,88]. However, our comparative assessment of bioclimatic, abiotic and anthropogenic parameters establishes a new baseline for understanding the refugee status, environmental niche, extinction vulnerability, and management requirements of *N. nasutus*.

Sites where *N. nasutus* formerly occurred do not differ from background points across the same region in landscape structure (elevation or slope). Furthermore, Wumingshan, where the species was extirpated before the recent historical period, has lower elevation, lower slope, and a different range of bioclimatic parameters (greater temperature seasonality, reduced diurnal temperature range, reduced precipitation indices and seasonality) compared to sites where the species persisted within living memory. These differences are shown by statistical comparisons and/or by the greatest loadings for PC1 in our PCA, where Wumingshan is clearly differentiated from all other sites. These findings demonstrate that *N. nasutus* formerly occurred over a much wider range of bioclimatic and abiotic conditions, and thus potentially constitutes a landscape-generalist species. In contrast, our statistical and PCA results show Bangliang-Trung Khanh represents a high-elevation refugium (higher elevation and slope) within the species' former range, and is also significantly more inaccessible in terms of both elevation and slope compared to all sites where local *N. nasutus* populations have been extirpated. Conversely, Bangliang-Trung Khanh is no different in bioclimatic parameters compared to sites where the species has been lost, indicating the importance of local landscape structure for providing an ecological refuge. This finding is supported by spatial relationships between gibbon records and GHF, with *N. nasutus* lost from all sites where local human pressures are typical for the wider region, and only surviving at a site with significantly low GHF, which is likely correlated with local landscape inaccessibility.

These findings demonstrate that the dynamic biogeography of past population decline in *N. nasutus* is comparable to that of many other threatened species [5–9], including Chinese gibbons [17,89], which were former landscape generalists but now persist only as high-elevation refugee populations. Previous studies of historical gibbon and other mammalian extinction dynamics demonstrate that extinctions across eastern and southeast Asia show strong spatial structuring, indicating that population persistence or loss was regulated by anthropogenic pressures that spread directionally across the region [90]. Multiple species, including other regionally extirpated mammals present in the Wumingshan deposit [18,19], experienced progressive range contraction towards the southwest in response to a 'wavefront' of human demographic expansion associated with increased forest loss and hunting [88]. However, at the finer geographic scale of our study region, *N. nasutus* populations show no obvious spatial pattern of survival or loss across sites, suggesting that local-scale persistence is further regulated by specific landscape and environmental parameters. Similar patterns of complex regional decline, fragmentation and isolation are also seen in several other species, including gibbons, in other systems, and reflect the distribution of specific refugial conditions that limit local human access [89,91,92].

Our results provide important further insights into the conditions required for persistence of threatened populations. In comparison to other historical *N. nasutus* sites, which vary in their local geology, the Bangliang-Trung Khanh and Wumingshan landscapes both consist entirely of limestone (figure 1). This landscape structure is thought to have contributed to site inaccessibility and gibbon survival at Bangliang-Trung Khanh [30], which is differentiated from other gibbon localities along PC2 partly on the basis of presence of carbonate sedimentary rock. Similar karst systems are known to act as important refugia for populations of many other species across southeast Asia [93]. However, the geologically similar landscape at Wumingshan lost its gibbons before recent history, indicating that the structural features of limestone landforms alone are insufficient to ensure gibbon survival within human-occupied systems. Instead, a combination of landscape characteristics (higher elevation and slope as well as suitable geological landforms) may be required to occur together to support local gibbon persistence in the absence of conservation management.

Together, our analyses provide a new baseline for considering conservation actions for *N. nasutus*. Bangliang-Trung Khanh does not differ bioclimatically from other sites that historically supported gibbons, so it does not obviously represent suboptimal niche space in regard to these environmental parameters. However, the site is at the upper margin of the species' elevational range, and elevation influences key ecological characteristics of tropical forests (e.g. net primary productivity) in potentially complex ways [94]. We recommend further investigation into potentially atypical behavioural, ecological or demographic characteristics (e.g. group size, home range size) exhibited by *N. nasutus* at Bangliang-Trung Khanh associated with persistence under high-elevation conditions [95]. In terms of wider-scale conservation planning, modern-day data alone would suggest there are few suitable sites left across the species' former range that share key environmental characteristics with Bangliang-Trung Khanh (only 1.8% of background points have a comparable set of elevation, slope and GHF threshold values), meaning that few other places might thus be able to support another population. However, older records reveal a much greater range of environmental tolerances and potential conservation

landscapes across the species' former extent of occurrence, raising the possibility of population restoration through translocation to other suitable sites. This is an important concern, as the Bangliang-Trung Khanh population may be approaching the site's carrying capacity, necessitating evidence-based identification of novel conservation solutions to aid species recovery by increasing population size and distribution [96]. Past ecological baselines also indicate that *N. nasutus* may have the capacity for greater resilience to climatic change than suggested by modern-only data, although this requires further investigation through modelling habitat and resource shifts (e.g. in key food plants [97]) and associated changes in landscape use by local communities.

4.3. Conclusions

Our multidisciplinary approach, comprising morphometric and ecological investigations of past and present specimens and data, establishes a new perspective on niche requirements and population change for one of the world's rarest mammals and highlights potential new directions for its conservation. We recommend the adoption of similar combined methods to generate novel conservation evidence for other threatened species using subfossil and zooarchaeological material. Through this approach, we encourage wider integration of environmental archives into modern biodiversity research and management under the emerging discipline of conservation palaeobiology [98], in recognition of the urgent need to expand the conservation toolkit in order to mitigate the global extinction crisis.

Ethics. This work did not require ethical approval from a human subject or animal welfare committee.

Data accessibility. Morphometric landmark data used in this study are available online at University College London's Research Data Repository. All additional data are provided in the electronic supplementary material.

Declaration of AI use. We have not used AI-assisted technologies in creating this article.

Authors' contributions. S.T.T.: conceptualization, data curation, funding acquisition, methodology, project administration, resources, supervision, visualization, writing—original draft; A.O.: data curation, formal analysis, methodology, visualization, writing—review and editing; M.G.: formal analysis, methodology, visualization, writing—review and editing; S.B.: data curation, formal analysis, investigation, methodology, supervision, writing—review and editing; R.H.: formal analysis, investigation, methodology; Q.Y.: investigation, project administration, resources; T.A.N.: data curation, resources; L.B.: investigation, methodology, writing—review and editing; H.M.: investigation, project administration; J.H.: methodology, supervision; T.B.: investigation, methodology; H.C.: data curation, methodology, writing—review and editing; P.F.: validation, writing—review and editing; X.C.: conceptualization, data curation, funding acquisition, investigation, methodology, writing—review and editing.

All authors gave final approval for publication and agreed to be held accountable for the work performed therein.

Conflict of interest declaration. We declare we have no competing interests.

Funding. This study was supported by the China Scholarship Council (202106865003), the Arcus Foundation (G-PGM-2301-3885) and Research England.

Acknowledgements. We thank Liyun Wang (Chongzuo Zhuang Ethnological Museum) for help with excavations at Wumingshan, and all museum staff for enabling us to obtain comparative data from their hylobatid collections.

References

1. Salafsky N *et al*. 2019 Defining and using evidence in conservation practice. *Conserv. Sci. Pract.* **1**, e27. (doi:10.1111/csp2.27)
2. Bonebrake TC, Christensen J, Boggs CL, Ehrlich PR. 2010 Population decline assessment, historical baselines, and conservation. *Conserv. Lett*. **3**, 371–378. (doi:10.1111/j.1755-263x.2010.00139.x)
3. Mihoub JB, Henle K, Titeux N, Brotons L, Brummitt NA, Schmeller DS. 2017 Setting temporal baselines for biodiversity: the limits of available monitoring data for capturing the full impact of anthropogenic pressures. *Sci. Rep*. **7**, 41591. (doi:10.1038/srep41591)
4. Turvey ST, Crees JJ. 2019 Extinction in the Anthropocene. *Curr. Biol*. **29**, R982–R986. (doi:10.1016/j.cub.2019.07.040)
5. Kerley GIH, te Beest M, Cromsigt JPGM, Pauly D, Shultz S. 2020 The Protected Area Paradox and refugee species: the giant panda and baselines shifted towards conserving species in marginal habitats. *Conserv. Sci. Pract*. **2**, e203. (doi:10.1111/csp2.203)
6. Britnell JA, Zhu Y, Kerley GIH, Shultz S. 2023 Ecological marginalization is widespread and increases extinction risk in mammals. *Proc. Natl Acad. Sci. USA* **120**, e2205315120. (doi:10.1073/pnas.2205315120)
7. Fisher DO. 2011 Trajectories from extinction: where are missing mammals rediscovered? *Glob. Ecol. Biogeogr*. **20**, 415–425. (doi:10.1111/j.1466-8238.2010.00624.x)
8. Lea JM, Kerley GI, Hrabar H, Barry TJ, Shultz S. 2016 Recognition and management of ecological refugees: a case study of the Cape mountain zebra. *Biol. Conserv*. **203**, 207–215. (doi:10.1016/j.biocon.2016.09.017)

9. Tomlinson S *et al*. 2024 Ecological dynamics of moa extinctions reveal convergent refugia that today harbour flightless birds. *Nat. Ecol. Evol*. **8**, 1472–1481. (doi:10.1038/s41559-024-02449-x)
10. Monsarrat S, Novellie P, Rushworth I, Kerley G. 2019 Shifted distribution baselines: neglecting long-term biodiversity records risks overlooking potentially suitable habitat for conservation management. *Philos. Trans. R. Soc. B* **374**, 20190215. (doi:10.1098/rstb.2019.0215)
11. Smith KJ, Pierson JC, Evans MJ, Gordon IJ, Manning AD. 2024 Continental-scale identification and prioritisation of potential refugee species; a case study for rodents in Australia. *Ecography* **2024**, e07035. (doi:10.1111/ecog.07035)
12. Crees JJ, Collen B, Turvey ST. 2019 Bias, incompleteness and the 'known unknowns' in the Holocene faunal record. *Philos. Trans. R. Soc. B* **374**, 20190216. (doi:10.1098/rstb.2019.0216)
13. Kemp TS. 1999 *Fossils and evolution*. Oxford, UK: Oxford University Press.
14. Hughes AC. 2017 Understanding the drivers of Southeast Asian biodiversity loss. *Ecosphere* **8**, e01624. (doi:10.1002/ecs2.1624)
15. Wen R. 2009 *The distributions and changes of rare wild animals in China*. Chongqing, China: Chongqing Science and Technology Press.
16. Turvey ST, Crees JJ, Li Z, Bielby J, Yuan J. 2017 Long-term archives reveal shifting extinction selectivity in China's postglacial mammal fauna. *Proc. R. Soc. B* **284**, 20171979. (doi:10.1098/rspb.2017.1979)
17. Turvey ST, Crees JJ, Di Fonzo MMI. 2015 Historical data as a baseline for conservation: reconstructing long-term faunal extinction dynamics in Late Imperial–modern China. *Proc. R. Soc. B* **282**, 20151299. (doi:10.1098/rspb.2015.1299)
18. Turvey ST, Hansford J, Brace S, Mullin V, Gu S, Sun G. 2016 Holocene range collapse of giant muntjacs and pseudo-endemism in the Annamite large mammal fauna. *J. Biogeogr*. **43**, 2250–2260. (doi:10.1111/jbi.12763)
19. Stimpson CM, Utting B, O'Donnell S, Huong NTM, Kahlert T, Manh BV, Khanh PS, Rabett RJ. 2019 An 11 000-year-old giant muntjac subfossil from northern Vietnam: implications for past and present populations. *R. Soc. Open Sci*. **6**, 181461. (doi:10.1098/rsos.181461)
20. Stimpson CM, O'Donnell S, Huong NTM, Holmes R, Utting B, Kahlert T, Rabett RJ. 2021 Confirmed archaeological evidence of water deer in Vietnam: relics of the Pleistocene or a shifting baseline? *R. Soc. Open Sci*. **8**, 210529. (doi:10.1098/rsos.210529)
21. IUCN. 2024 The IUCN Red List of Threatened Species. *Version 2024-1*. See https://www.iucnredlist.org.
22. Fan P. 2017 The past, present, and future of gibbons in China. *Biol. Conserv.* **210B**, 29–39. (doi:10.1016/j.biocon.2016.02.024)
23. Turvey ST, Bruun K, Ortiz A, Hansford J, Hu S, Ding Y, Zhang T, Chatterjee HJ. 2018 New genus of extinct Holocene gibbon associated with humans in Imperial China. *Science* **360**, 1346–1349. (doi:10.1126/science.aao4903)
24. Ortiz A, Pilbrow V, Villamil CI, Korsgaard JG, Bailey SE, Harrison T. 2015 The taxonomic and phylogenetic affinities of *Bunopithecus sericus*, a fossil hylobatid from the Pleistocene of China. *PLoS One* **10**, e0131206. (doi:10.1371/journal.pone.0131206)
25. Ortiz A *et al*. 2019 Morphometric analysis of fossil hylobatid molars from the Pleistocene of southern China. *Anthropol. Sci*. **127**, 109–121. (doi:10.1537/ase.190331)
26. Tan B. 1985 The status of primates in China. *Primate Conserv.* **5**, 63–81.
27. Chan BPL, Tan X, Tan W. 2008 Rediscovery of the Critically Endangered eastern black crested gibbon *Nomascus nasutus* (Hylobatidae) in China, with preliminary notes on population size, ecology and conservation status. *Asian Primat. J.* **1**, 17–25.
28. Rawson BM, Insua-Cao P, Ha NM, Thinh VN, Duc HM, Mahood S, Geissmann T, Roos C. 2011 *The conservation status of gibbons in Vietnam*. Hanoi, Vietnam: Fauna & Flora International/Conservation International.
29. Geissmann T, Dang NX, Lormée N, Momberg F. 2000 *Vietnam primate conservation status review 2000. Part 1: gibbons*. Hanoi, Vietnam: Fauna & Flora International, Indochina Programme.
30. Wearn OR, Raghavan R, Nguyen Minh P, Nguyen Duc T, Wu H, Zhang Z, Trinh Dinh H, Fan P, Ma C. 2021 *Conservation action plan for the cao vit gibbon (Nomascus nasutus) 2021-2030 with a vision to 2050*. Hanoi, Vietnam: Fauna & Flora International – Vietnam Programme/IUCN SSC Conservation Planning Specialist Group.
31. Wearn OR *et al*. 2024 Vocal fingerprinting reveals a substantially smaller global population of the Critically Endangered cao vit gibbon (*Nomascus nasutus*) than previously thought. *Sci. Rep*. **14**, 416. (doi:10.1038/s41598-023-50838-2)
32. Guangxi Institute of Cultural Relics Protection and Archaeology. 2021 *An archaeological report of Huashan in Zuojiang River basin (2013-2016)*. Beijing, China: Cultural Relics Press.
33. Chen X, Yang Q, Jiangzuo Q. 2019 Guǎngxī Zuǒjiāng liúyù xīnshíqì shídài bèi qiū yízhǐ dòngwù kǎogǔxué yánjiū. *Cult. Relics S. China* **2**, 155–164.
34. Dabney J *et al*. 2013 Complete mitochondrial genome sequence of a middle Pleistocene cave bear reconstructed from ultrashort DNA fragments. *Proc. Natl Acad. Sci. USA* **110**, 15758–15763. (doi:10.1073/pnas.1314445110)
35. Meyer M, Kircher M. 2010 Illumina sequencing library preparation for highly multiplexed target capture and sequencing. *Cold Spring Harb. Protoc*. **2010**, pdb.prot5448.(doi:10.1101/pdb.prot5448)
36. Kircher M, Sawyer S, Meyer M. 2012 Double indexing overcomes inaccuracies in multiplex sequencing on the Illumina platform. *Nucleic Acids Res.* **40**, e3. (doi:10.1093/nar/gkr771)
37. Henriksen RA, Woods R, Barnes I, Kennerley RJ, Borroto-Páez R, Brace S, Turvey ST. 2024 Genomics of historical museum collections clarifies species diversity in Cuban hutias (*Capromys*). *J. Mammal.* **105**, 1365–1377. (doi:10.1093/jmammal/gyae090)
38. Swindler DR. 2002 *Primate dentition: an introduction to the teeth of non-human primates*. Cambridge, UK: Cambridge University Press.
39. Kozakowski SA. 2013 *3D geometric morphometric analysis of hylobatid cranial ontogeny: implications for interpreting the evolutionary history of hominoid cranial growth*. PhD thesis, University of Toronto.
40. Wood BA, Abbott SA. 1983 Analysis of the dental morphology of Plio-Pleistocene hominids. I. Mandibular molars: crown area measurements and morphological traits. *J. Anat*. **136**, 197–219.

41. Wood BA, Engleman CA. 1988 Analysis of the dental morphology of Plio-Pleistocene hominids. V. Maxillary postcanine tooth morphology. *J. Anat*. **161**, 1–35.
42. Benazzi S *et al*. 2012 Cervical and crown outline analysis of worn Neanderthal and modern human lower second deciduous molars. *Am. J. Phys. Anthropol*. **149**, 537–546. (doi:10.1002/ajpa.22155)
43. Burnett SE, Irish JD, Fong MR. 2013 Wear's the problem? Examining the effect of dental wear on studies of crown morphology. In *Anthropological perspectives on tooth morphology* (eds GR Scott, JD Irish), pp. 535–554. Cambridge, UK: Cambridge University Press. (doi:10.1017/cbo9780511984464.021)
44. Dykes SJ, Pilbrow VC. 2019 A mathematical landmark-based method for measuring worn molars in hominoid systematics. *PeerJ* **7**, e6990. (doi:10.7717/peerj.6990)
45. Molnar S. 1971 Human tooth wear, tooth function and cultural variability. *Am. J. Phys. Anthropol*. **34**, 175–189. (doi:10.1002/ajpa.1330340204)
46. Bailey SE, Benazzi S, Buti L, Hublin J -J. 2016 Allometry, merism, and tooth shape of the lower second deciduous molar and first permanent molar. *Am. J. Phys. Anthropol*. **159**, 93–105. (doi:10.1002/ajpa.22842)
47. Gilbert CC, Ortiz A, Pugh KD, Campisano CJ, Patel BA, Singh NP, Fleagle JG, Patnaik R. 2020 New Middle Miocene ape (Primates: Hylobatidae) from Ramnagar, India fills major gaps in the hominoid fossil record. *Proc. R. Soc. B* **287**, 20201655. (doi:10.1098/rspb.2020.1655)
48. Cooke SB, Terhune CE. 2015 Form, function, and geometric morphometrics. *Anat. Rec*. **298**, 5–28. (doi:10.1002/ar.23065)
49. Rohlf FJ. 2015 The Tps series of software. *Hystrix* **26**, 9–12. (doi:10.4404/hystrix-26.1-11264)
50. Bookstein FL. 1992 *Morphometric tools for landmark data: geometry and biology*. Cambridge, UK: Cambridge University Press.
51. Gómez-Robles A, Bermúdez de Castro JM, Martinón-Torres M, Prado-Simón L, Arsuaga JL. 2015 A geometric morphometric analysis of hominin lower molars: evolutionary implications and overview of postcanine dental variation. *J. Hum. Evol*. **82**, 34–50. (doi:10.1016/j.jhevol.2015.02.013)
52. Pitirri MK, Begun D. 2019 A new method to quantify mandibular corpus shape in extant great apes and its potential application to the hominoid fossil record. *Am. J. Phys. Anthropol*. **168**, 318–328. (doi:10.1002/ajpa.23749)
53. Gunz P, Mitteroecker P, Bookstein FL. 2005 Semilandmarks in three dimensions. In *Modern morphometrics in physical anthropology* (ed. DE Slice), pp. 73–98. New York, NY: Springer.
54. Klingenberg CP. 2011 MorphoJ: an integrated software package for geometric morphometrics. *Mol. Ecol. Resour*. **11**, 353–357. (doi:10.1111/j.1755-0998.2010.02924.x)
55. Hammer Ø, Harper DAT, Ryan PD. 2001 PAST: paleontological statistics software package for education and data analysis. *Palaeontol. Electron.* **4**, 4.
56. R Development Core Team. 2010 R: a language and environment for statistical computing. Vienna, Austria: R Foundation for statistical computing.
57. Adams DC, Otárola-Castillo E. 2013 geomorph: an R package for the collection and analysis of geometric morphometric shape data. *Methods Ecol. Evol*. **4**, 393–399. (doi:10.1111/2041-210x.12035)
58. Schlager S, Jefferis G, Dryden I. 2017 Morpho: calculations and visualisations related to geometric morphometrics. *R package*.
59. Geissmann T, Cuong NT. 2009 *Results of a rapid gibbon survey in the Lung Ri area (Trung Khanh District, Cao Bang Province) in northeastern Vietnam*. Hanoi, Vietnam: Fauna and Flora International, Vietnam Programme.
60. Fick SE, Hijmans RJ. 2017 WorldClim 2: new 1-km spatial resolution climate surfaces for global land areas. *Int. J. Climatol*. **37**, 4302–4315. (doi:10.1002/joc.5086)
61. Brown JL, Hill DJ, Dolan AM, Carnaval AC, Haywood AM. 2018 PaleoClim, high spatial resolution paleoclimate surfaces for global land areas. *Sci. Data* **5**, 180254. (doi:10.1038/sdata.2018.254)
62. Reuter HI, Nelson A, Jarvis A. 2007 An evaluation of void-filling interpolation methods for SRTM data. *Int. J. Geogr. Inf. Sci*. **21**, 983–1008. (doi:10.1080/13658810601169899)
63. Hartmann J, Moosdorf N. 2012 The new global lithological map database GLiM: a representation of rock properties at the Earth surface. *Geochem. Geophys. Geosyst.* **13**, Q12004. (doi:10.1029/2012GC004370)
64. WCS & CIESIN. 2005 *Last of the Wild project, version 2: Global Human Footprint dataset (geographic)*. New York, NY: NASA Socioeconomic Data and Applications Center.
65. Carbone L *et al*. 2014 Gibbon genome and the fast karyotype evolution of small apes. *Nature* **513**, 195–201. (doi:10.1038/nature13679)
66. Thinh VN *et al*. 2010 Mitochondrial evidence for multiple radiations in the evolutionary history of small apes. *BMC Evol. Biol*. **10**, 74. (doi:10.1186/1471-2148-10-74)
67. Chivers DJ, Anandam MV, Groves CP, Molur S, Rawson BM, Richardson MC, Roos C, Whittaker D. 2013 Family Hylobatidae (gibbons). In *Handbook of the mammals of the world, volume 3: primates* (eds RA Mittermeier, AB Rylands, DE Wilson), pp. 754–791, vol. 3. Barcelona, Spain: Lynx Edicions.
68. Roos C. 2016 Phylogeny and classification of gibbons (Hylobatidae). In *Evolution of gibbons and siamang: phylogeny, morphology, and cognition* (eds U Reichard, H Hirai, C Barelli), pp. 151–165. New York, NY: Springer. (doi:10.1007/978-1-4939-5614-2_7)
69. Fan P *et al*. 2017 Description of a new species of *Hoolock* gibbon (Primates: Hylobatidae) based on integrative taxonomy. *Am. J. Primatol*. **79**, e22631. (doi:10.1002/ajp.22631)
70. Groves C. 2001 *Primate taxonomy*. Washington, DC: Smithsonian Institution Press.
71. Fleagle JG. 2013 *Primate adaptation and evolution,* 3rd edn. San Diego, CA: Elsevier.

72. Meloro C, Cáceres NC, Carotenuto F, Sponchiado J, Melo GL, Passaro F, Raia P. 2015 Chewing on the trees: constraints and adaptation in the evolution of the primate mandible. *Evolution* **69**, 1690–1700. (doi:10.1111/evo.12694)
73. Gamarra B, Nova Delgado M, Romero A, Galbany J, Pérez-Pérez A. 2016 Phylogenetic signal in molar dental shape of extant and fossil catarrhine primates. *J. Hum. Evol*. **94**, 13–27. (doi:10.1016/j.jhevol.2016.01.005)
74. Delgado MN, Galbany J, Górka K, Pérez-Pérez A. 2015 Taxonomic implications of molar morphology variability in capuchins. *Int. J. Primatol*. **36**, 707–727. (doi:10.1007/s10764-015-9850-4)
75. Nova Delgado M, Galbany J, Pérez-Pérez A. 2016 Molar shape variability in platyrrhine primates. *J. Hum. Evol*. **99**, 79–92. (doi:10.1016/j.jhevol.2016.07.006)
76. Avià Y, Romero A, Estebaranz-Sánchez F, Pérez-Pérez A, Cuesta-Torralvo E, Martínez LM. 2022 Dental topography and dietary specialization in Papionini primates. *Front. Ecol. Evol*. **10**, 969007. (doi:10.3389/fevo.2022.969007)
77. Guan Z, Ma C, Fei H, Huang B, Ning W, Ni Q, Jiang X, Fan P. 2018 Ecology and social system of northern gibbons living in cold seasonal forests. *Zool. Res.* **39**, 255–265. (doi:10.24272/j.issn.2095-8137.2018.045)
78. Palombit RA. 1997 Inter- and intraspecific variation in the diets of sympatric siamang (*Hylobates syndactylus*) and lar gibbons (*Hylobates lar*). *Folia Primatol*. **68**, 321–337. (doi:10.1159/000157260)
79. Elder AA. 2009 Hylobatid diets revisited: the importance of body mass, fruit availability, and interspecific competition. In *The gibbons* (eds D Whittaker, S Lappan), pp. 133–159. New York, NY: Springer. (doi:10.1007/978-0-387-88604-6_8)
80. Pilbrow V. 2007 Patterns of molar variation in great apes and their implications for hominin taxonomy. In *Dental perspectives on human evolution: state of the art research in dental paleoanthropology* (eds SE Bailey, JJ Hublin), pp. 9–32. Dordrecht, The Netherlands: Springer. (doi:10.1007/978-1-4020-5845-5_2)
81. Frisch JE. 1973 The hylobatid dentition. In *Gibbon and siamang* (eds H Preuschoft, JD Chivers, WY Brockelman, N Creel), pp. 55–95, vol. II. Basel, Switzerland: Karger.
82. Jablonski NG, Chaplin G. 2009 The fossil record of gibbons. In *The gibbons: new perspectives on small ape socioecology and population biology* (eds D Whittaker, S Lappan), pp. 111–130. New York, NY: Springer. (doi:10.1007/978-0-387-88604-6_7)
83. Ravosa MJ. 1991 Structural allometry of the prosimian mandibular corpus and symphysis. *J. Hum. Evol*. **20**, 3–20.
84. Ravosa MJ. 2000 Size and scaling in the mandible of living and extinct apes. *Folia Primatol*. **71**, 305–322. (doi:10.1159/000021754)
85. Delgado MN, Gamarra B, Nadal J, Mercadal O, Olesti O, Guàrdia J, Pérez-Pérez A, Galbany J. 2015 Dental shape variability in cercopithecoid primates: a model for the taxonomic attribution of macaques from Roman archaeological contexts. *Folia Primatol*. **85**, 361–378. (doi:10.1159/000371633)
86. Cardini A, Elton S, Kovarovic K, Strand Viðarsdóttir U, Polly PD. 2021 On the misidentification of species: sampling error in primates and other mammals using geometric morphometrics in more than 4000 individuals. *Evol. Biol*. **48**, 190–220. (doi:10.1007/s11692-021-09531-3)
87. Reichard UH, Croissier MM. 2016 Hylobatid evolution in paleogeographic and paleoclimatic context. In *Evolution of gibbons and siamang: phylogeny, morphology, and cognition* (eds U Reichard, H Hirai, C Barelli), pp. 111–135. New York, NY: Springer. (doi:10.1007/978-1-4939-5614-2_5)
88. Marks RB. 2017 *China: an environmental history,* 2nd edn. Lanham, MD: Rowman & Littlefield.
89. Yang L, Shi K, Ma C, Ren G, Fan P. 2021 Mechanisms underlying altitudinal and horizontal range contraction: the western black crested gibbon. *J. Biogeogr*. **48**, 321–331. (doi:10.1111/jbi.13998)
90. Channell R, Lomolino MV. 2000 Dynamic biogeography and conservation of endangered species. *Nature* **403**, 84–86. (doi:10.1038/47487)
91. González LM. 2015 Prehistoric and historic distributions of the Critically Endangered Mediterranean monk seal (*Monachus monachus*) in the eastern Atlantic. *Mar. Mammal Sci*. **31**, 1168–1192. (doi:10.1111/mms.12228)
92. Reside AE *et al*. 2019 Persistence through tough times: fixed and shifting refuges in threatened species conservation. *Biodivers. Conserv*. **28**, 1303–1330. (doi:10.1007/s10531-019-01734-7)
93. Clements R, Sodhi NS, Schilthuizen M, Ng PKL. 2006 Limestone karsts of southeast Asia: imperiled arks of biodiversity. *Bioscience* **56**, 733. (doi:10.1641/0006-3568(2006)56[733:LKOSAI]2.0.CO;2)
94. Chen X, Zhang Y. 2023 Impacts of climate, phenology, elevation and their interactions on the net primary productivity of vegetation in Yunnan, China under global warming. *Ecol. Indic*. **154**, 110533. (doi:10.1016/j.ecolind.2023.110533)
95. Bryant JV, Olson VA, Chatterjee HJ, Turvey ST. 2015 Identifying environmental versus phylogenetic correlates of behavioural ecology in gibbons: implications for conservation management of the world's rarest ape. *BMC Evol. Biol*. **15**, 171. (doi:10.1186/s12862-015-0430-1)
96. Fan P, Ren G, Wang W, Scott M, Ma C, Fei H, Wang L, Xiao W, Zhu J. 2013 Habitat evaluation and population viability analysis of the last population of cao vit gibbon (*Nomascus nasutus*): implications for conservation. *Biol. Conserv*. **161**, 39–47. (doi:10.1016/j.biocon.2013.02.014)
97. Fan P, Fei H, Scott M, Zhang W, Ma C. 2011 Habitat and food choice of the Critically Endangered cao vit gibbon (*Nomascus nasutus*) in China: implications for conservation. *Biol. Conserv*. **144**, 2247–2254. (doi:10.1016/j.biocon.2011.05.016)
98. Kiessling W, Raja NB, Roden VJ, Turvey ST, Saupe EE. 2019 Addressing priority questions of conservation science with palaeontological data. *Phil. Trans. R. Soc. B* **374**, 20190222. (doi:10.1098/rstb.2019.0222)